Numerical Study of Balearic Meteotsunami Generation and Propagation under Synthetic Gravity Wave Forcing [PRE-PRINT OF THE OCEAN MODELLING PUBLICATION http://dx.doi.org/10.1016/j.ocemod.2017.02.001]

Matjaž Ličer[a,b,*], Baptiste Mourre[a], Charles Troupin[a], Andreas Krietemeyer[a], Agusti Jansá[d], Joaquín Tintoré[a,c]

[a]*SOCIB, Balearic Islands Coastal Observing and Forecasting System, Parc Bit, Edifici Naorte, 07121 Palma, Spain*
[b]*National Institute of Biology, Marine Biology Station, Fornače 41, 6330 Piran, Slovenia*
[c]*IMEDEA (CSIC-UIB), c/ Miquel Marques 21, 07190 Esporles, Spain*
[d]*UIB, Department of Physics, Carretera de Valldemossa, km 7.5, 07122 Palma de Mallorca, Spain*

Abstract

We use a high resolution nested ocean modelling system forced by synthetic atmospheric gravity waves to investigate Balearic meteotsunami generation, amplification and propagation properties. We determine how meteotsunami amplitude outside and inside of the Balearic port of Ciutadella depends on forcing gravity wave direction, speed and trajectory. We quantify the contributions of Mallorca shelves and Menorca Channel for different gravity wave forcing angles and speeds. The Channel is demonstrated to be the key build-up region determining meteotsunami amplitude in Ciutadella while northern and southern Mallorca shelves serve mostly as barotropic wave guides but do not significantly contribute to seiche amplitude in Ciutadella. This fact seriously reduces early-warning alert times in cases of locally generated pressure perturbations. We track meteotsunami propagation paths in the Menorca Channel for several forcing velocities and show that the Channel bathymetry serves as a focusing lens for meteotsunami waves whose paths are constrained by the forcing direction.

*Corresponding author:
Email address: `matjaz.licer@nib.si` (Matjaž Ličer)

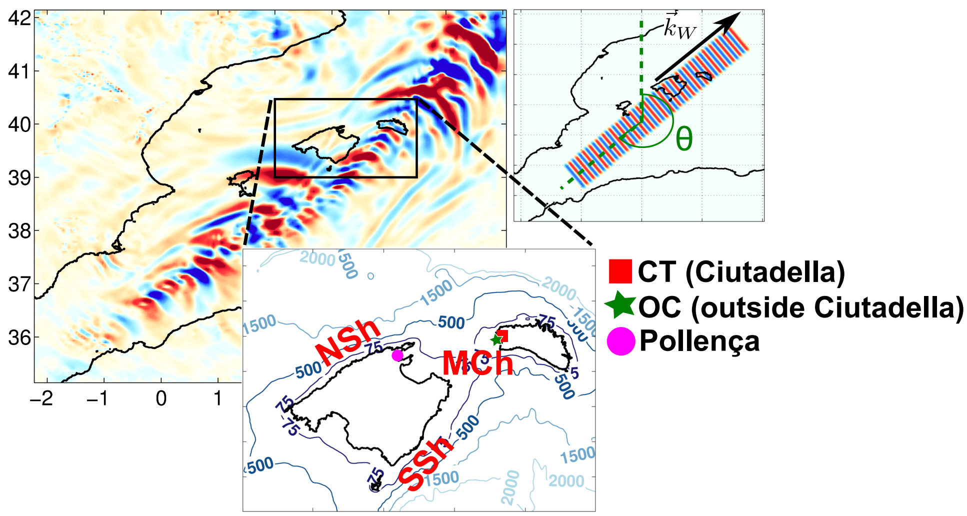

Figure 1: Background left: BRIFS operational WRF model high-pass filtered air pressure wave on the 11 June 2015 (color scale is truncated at ±0.3 hPa). Black box, zoomed-up in the inset: ROMS parent domain with the Balearic bathymetry contours in meters with marked northern shelf (NSh), southern shelf (SSh) and Menorca Channel (MCh). Tiny red square in the inset shows ROMS child domain over the Ciutadella harbour. Green star shows the location of interest outside the Ciutadella harbour (denoted as OC in the rest of the paper). Purple circle shows location of the town of Pollença, Mallorca. Top right: synthetic air pressure snapshot for the $\theta = 230^{\circ}$ incident angle.

We show that faster meteotsunamis propagate over deeper ocean regions, as required by Proudman resonance. We estimate meteotsunami speed under sub- and supercritical forcing and derive a first order estimate of its magnitude. We show that meteotsunamis, generated by supercritical gravity waves, propagate with a velocity which is equal to an arithmetic mean of the forcing velocity and local barotropic ocean wave speed.

Keywords: meteotsunami modelling, meteotsunami propagation, Proudman resonance, meteotsunami amplification

---

1. Introduction

Meteotsunamis, i.e. tsunamis of meteorological origin [1, 2], are ocean waves in the tsunami frequency band generated over open ocean by the high frequency air pressure modulations of atmospheric gravity waves, convective pressure jumps or other kinds of atmospheric instabilities [1, 3]. Their amplification mechanisms include Proudman resonance (the matching of the air pressure disturbance velocity U and local ocean barotropic velocity $c_b = \sqrt{gH}$), topographic amplifications over continental shelves and harbour resonances as ocean waves enter narrow bays and inlets, oscillating at frequencies close to the resonant frequencies of these partially enclosed basins. These processes have been thoroughly explained elsewhere, e.g. [1, 4, 5]. Meteotsunamis have been observed all over the world oceans and their destructive port oscillations can also be found in the Mediterranean, for instance in the Balearic port of Ciutadella (see red square in the inset to Figure 1) [3, 6, 7, 8, 9, 10]. Here they are known as 'rissagas', but other examples can be found along the Sicilian and Croatian Adriatic coasts [11]. Meteotsunamis can even occur sequentially along the trajectory of the same synoptic system [4, 12].

Meteotsunami research efforts have been growing in the past decades and our understanding of the underlying processes has substantially improved. Nevertheless open issues remain. Even though Proudman resonance is known to play an important role in meteotsunami-related atmosphere-ocean energy transfer [13, 14, 15, 16], we still lack sufficient understanding of how a meteotsunami amplification is influenced by the resonant atmosphere-ocean interactions or by the local bathymetry, as was noted recently in [2]. In this paper we revisit this issue by presenting rissaga generation and propagation studies under synthetic forcing by atmospheric gravity waves, similar to the wave train modelled for June 11 2015, shown in Figure 1. Similar waves have previously been observed over the region [17, 18, 19]. Here we study the details of the respective contributions of the Mallorca shelves and Menorca Channel (see Figure 1 for location) to Ciutadella rissagas under gravity wave forcing conditions, and the role of Proudman resonance in determining the meteotsunami propagation paths over the shelves and the Menorca Channel. We conclude with an analysis of meteotsunami propagation speeds in the Menorca Channel during sub- and supercritical ($U > c_{b0}$) forcing regimes, where $c_{b0} \approx 27 - 28$ m s^{-1} is the Menorca Channel barotropic speed. The paper is organized as follows: Section 2.1 provides a brief description of the ocean modelling system. Section 2.2 describes synthetic atmospheric forcing used in the presented sensitivity analysis. Rissaga sensitivity on forcing speed and direction is described in Section 3.1, respective roles of the shelves and the Channel are presented in Section 3.2 and propagation speed analysis is contained in Section 3.3. This is followed by the conclusions in Section 4.

2. Modelling Setup

2.1. ROMS Model Configuration

The ocean modelling system used in this study is similar to that presented in [3], which is also the oceanic component of the Balearic Islands Rissaga Forecasting System (BRIFS) run operationally on a daily basis at SOCIB. It is based on a double grid configuration of the ROMS model [20] with a 10-m resolution grid around Ciutadella Inlet (hereafter child model) nested in a 1-km resolution grid encompassing Mallorca and Menorca Islands (hereafter parent model).

Both modeling domains are depicted in Figure 1. ROMS is a 3D free-surface, split-explicit primitive equation model with Boussinesq and hydrostatic approximations. Due to the 2-dimensional nature of the processes at play, the model uses homogeneous temperature and salinity as initial conditions. A quadratic parameterization is used for bottom drag. At the open lateral boundaries, Chapman and Flather conditions are used for free surface and 2D momentum respectively. While no external boundary input is used for the larger domain, the free surface and vertically integrated velocities of the parent model provide the lateral boundary conditions for the child model with a 2-minute temporal resolution. BRIFS features a full WRF atmospheric model component to provide realistic high resolution atmospheric forcing for ROMS (see Figure 1 for an illustration). Here, the simulations were forced by the 2-minute resolution synthetic atmospheric pressure fields, similar to realistic WRF outputs, to analyse in detail the impact of the gravity wave properties on ocean model response.

2.2. Synthetic Atmospheric Boundary Conditions

Pressure wave forcing fields, with parameters similar to existing observations ([17, 18], and SOCIB June 11 2015 mean sea level pressure observations, available online via SOCIB THREDDS server at http://thredds.socib.es-/thredds/catalog.html), were generated as follows. Each respective numerical experiment featured an atmospheric pressure wave travelling at a definite phase velocity U, incident angle θ and lateral arc width of 1°. Frequency ν_W was kept constant at 10^{-3} s^{-1} for all waves. This frequency implies a 16.7-minute period, corresponding to a Ciutadella harbour amplification factor of 2.6, see e.g. [5]. Note that the ground state eigenperiod of the Ciutadella harbour equals 10.5 minutes with a harbour amplification factor of 9.0. This paper does not address the sensitivity of the rissaga to the forcing frequency, which scales the final harbour resonance, but focuses on the generation, amplification and propagation processess over the shelves before entering Ciutadella inlet. The angle θ is stated throughout the paper using the nautical notation: $\theta = 180^\circ$ - wave propagates from the south, $\theta = 270^\circ$ - wave propagates from the west. For each numerical experiment a separate pressure wave was generated for angles from $\theta = 180^\circ$ to 270° in steps of 10° and with phase velocities from $U = 21$ m/s to 36 m/s in steps of 1 m/s. The atmospheric pressure wave is then generated with $p(\vec{r}, t) = p_0 \cdot R(t, t_R) \cdot \cos(\vec{k}_W \cdot \vec{r} - \omega_W t)$, where p_0 is the pressure wave amplitude (set to 3 hPa, matching past observed values and implying pressure change rates of about 0.7 hPa/min), $R(t, t_R)$ is a pressure amplitude ramp function which linearly rises from 0 to 1 as t grows from 0 to ramp time t_R (set to $t_R = 16$ minutes). The quantity $\vec{k}_W = (2\pi R_\oplus/\lambda_W)[\cos\theta, \sin\theta]$ is the wave-vector, $R_\oplus$ is the mean Earth radius, $\lambda_W = U/\nu_W$ is the pressure wave wavelength, $\vec{r} = [\lambda, \phi]$

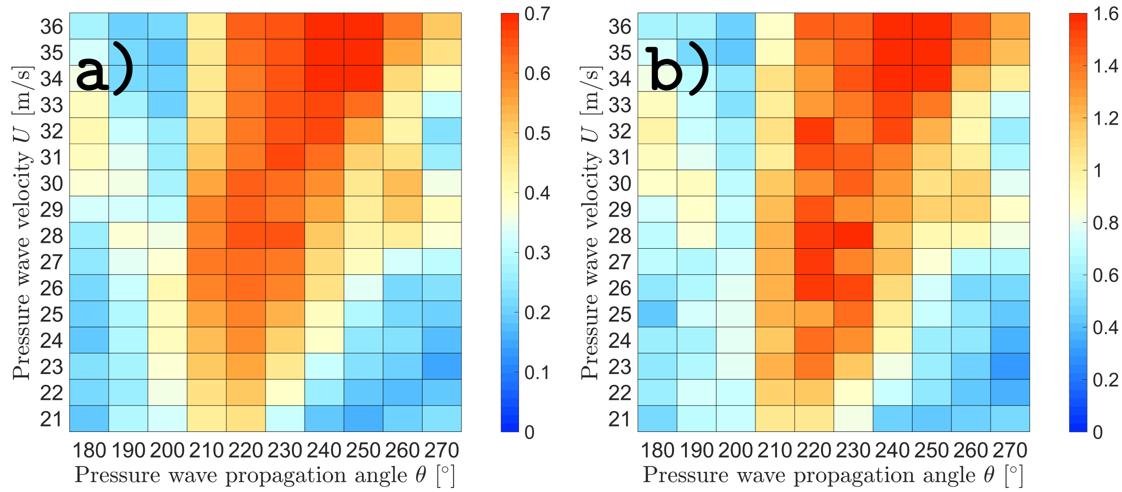

Figure 2: a) Dependence of the maximum generated SSH anomaly [m] at the OC point on the forcing gravity wave incident angle θ and its speed U. Colorbar depicts the elevation scale in meters. b) The same for the CT point inside Ciutadella harbour (see Figure 1 for location). Note the different color scales in both panels.

is the geo-referenced location on the Earth surface (λ and ϕ being longitude and latitude), $\omega_W = 2\pi\nu_W$ is the wave angular frequency and t is time. The pressure wave is then cropped in space and time to have the appropriate lateral width (0.5° to 1° arc degree) and duration (set to 6 hours - note that the gravity wave shown in Figure 1 endured for over 9 hours).

3. Results and Discussion

3.1. Rissaga Sensitivity to Pressure Wave Direction and Speed: the influence of Proudman resonance.

To test the reliability of the modelling system's physics we first ran a separate 24-hour simulation for each of the 160 forcing scenarios described in Section 2.2 to study how the SSH anomaly outside and inside Ciutadella harbour depends on two key parameters: pressure wave propagation angle θ and velocity U. These results are presented in Figure 2. Note that they are consistent with those from [6] even though our ocean model is forced by wave trains instead of a pressure step function as in [6] or [21]. Several features are present in Figure 2. First, both matrices, outside (left panel in Figure 2) and inside (right panel in Figure 2) Ciutadella harbour, exhibit the absence of significant rissagas for angles below $\theta = 210°$ and above $\theta = 260°$. Second, there is a wide interval of velocities, from 23 m/s to 36 m/s, which generate substantial rissagas for forcing angles $210° \leq \theta \leq 250°$. Third, there are two areas with maximum SSH anomalies, one at $\theta = 230°$ and $U = 28$ m/s, and another at $\theta = 240° - 250°$ and $U = 34 - 36$ m/s. And finally, the SSH anomaly pattern at the CT point, extracted from the ROMS child domain and depicted in the right panel in Figure 2, exhibits the same overall features as the one at OC point, taken from the ROMS parent model and depicted in the left panel in Figure 2, although some additional modulations (i.e. intensification of the ($\theta = 230°, 28$ m/s) maximum inside the harbour) are present.

In what follows we proceed to explain these features. To understand the absence of significant rissagas for angles below $\theta = 210°$ and above $\theta = 260°$, the left panel of Figure 3 is instrumental. The $\theta = 210°$ and $\theta = 260°$ incidence angles, plotted over the shallow water wave speed $\sqrt{gH}$, illustrate that the range of angles leading to significant rissagas in our simulations is linked with the orientation of Mallorca shelves and Menorca Channel. Within this cone of forcing directions, a large range of shallow water velocities is found along the propagating path of any given atmospheric disturbance towards Ciutadella. One of these velocities will match the forcing velocity giving rise to efficient transfer of energy from atmosphere to ocean through Proudman resonance.

The right panel of Figure 3 shows the Proudman length $L_P(\theta, U)$ dependence at the OC location on the forcing gravity wave incident angle θ and its speed U. Proudman length was computed in a similar fashion as suggested in [22]. It is defined as the total accumulated length (in kilometers) of the gravity wave path (propagating over the OC point at propagation angle θ) over which the Froude number $Fr = U/\sqrt{gH}$ is within 5 percent of its critical value, namely where $|Fr - 1| < 0.05$.

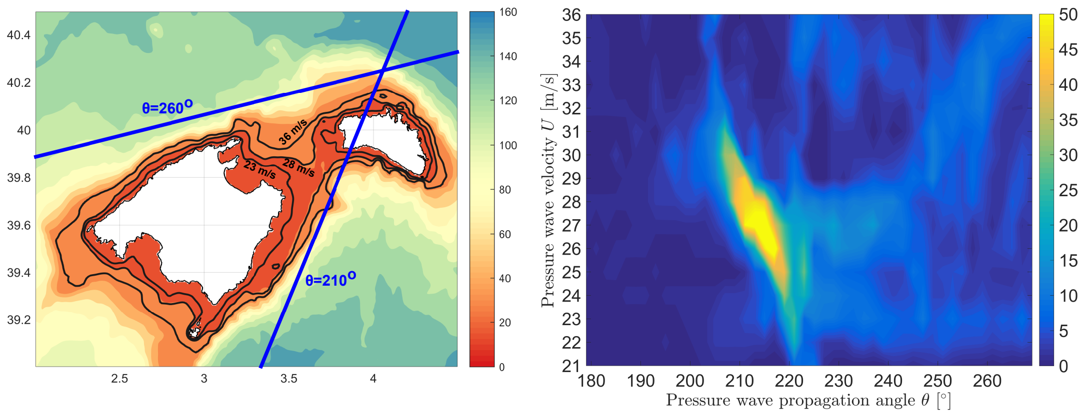

Figure 3: Left: Shallow water wave speed $\sqrt{gH}$ [m/s] over the model domain. Black contour lines denote 23 m/s (innermost line), 28 m/s and 36 m/s (outermost line) speed isolines. The blue lines denote directions of gravity wave propagations at angles $\theta = 210°$ and $\theta = 260°$. Right: Proudman length $L_P(\theta, U)$ matrix [km] computed for the OC point (see Figure 1 for exact location).

The Proudman length matrix indicates that gravity waves, which propagate through the OC point in straight lines at angles $210° - 220°$ and speeds $26 - 28$ m/s, are the ones which travel to the largest extent over suitable ocean depths for the Proudman resonance to occur. Propagation through the OC point at these angles can only take place over the Southern Mallorcan shelf and the Menorca Channel, as can be seen from the left panel in Figure 3. The local SSH anomaly maximum in Figure 2, which occurs at $\theta = 220 - 230°$ and $U = 26 - 28$ m/s, therefore seems a direct consequence of the Proudman resonance over the Southern Mallorcan shelf and the Menorca Channel. Since it is computed along straight lines, the Proudman length criterion is however insufficient to explain the wider pattern of high values of the SSH anomalies at OC and CT points (see Figure 2) between angles $\theta = 210°$ and $\theta = 260°$. To explain this wide range one must take into account how the broader shape of Balearic bathymetry impacts the propagation of the barotropic waves. As will be shown below in more detail, Balearic bathymetry acts as a focusing lens for meteotsunami waves while the shelves act as the guides for coastaly trapped edge waves. This is due to the fact that free waves in inhomogeneous media propagate in accordance with the Snell's law of refraction, which effectively states that travelling waves deflect toward regions with lower propagation velocity. Consequently the waves, generated by the forcing angles between $\theta = 210°$ and $\theta = 260°$, which would otherwise perhaps have missed Ciutadella, will be guided along the isobaths into the Channel and towards Ciutadella - this is also explicitely shown below in Section 3.3. Outside the $\theta = 210° - 260°$ region, the ocean is too deep for the Proudman resonance to occur since velocities of atmospheric disturbances rarely surpass 40 m/s.

As for the SSH anomaly peak around $U = 34 - 36$ m/s and $240° - 260°$: our simulations indicate that gravity waves at these speeds and angles generate energetic coastally trapped edge waves and excite Channel eigenmodes with periods of the order of a few hours (not shown in the paper). Edge waves propagate northeastward along the Mallorca shelves, enter the Channel along the isobaths and superimpose with the eigenmodes adding a final contribution to the SSH anomalies visible at OC and CT points. Note that the SSH matrix in [6], where a single pressure jump (modelled after the 2006 rissaga event) was employed for synthetic experiments, indicates no such response maximum at $U = 34 - 36$ m/s and $240° - 260°$ values. This further hints that the secondary maximum, visible in our Figure 2 at $U = 34 - 36$ m/s and $240° - 260°$, might be a consequence of forcing with gravity wave-trains of sufficient duration to excite edge waves which have enough energy to contribute to Ciutadella rissagas.

Finally, we attribute the modulation in amplitude at point CT, as compared to the point OC, to a modulation of the frequency of the first sea level oscillations reaching the entrance of Ciutadella inlet. Preliminary calculations shows these oscillations to be comprised between 13 and 17 minutes (not shown in the paper), directly affecting the amplification inside the inlet [5]. No particular distribution pattern was found over the range of forcing wave speeds and directions. These aspects remains out of the scope of the present paper and further investigation is needed to better understand these processes.

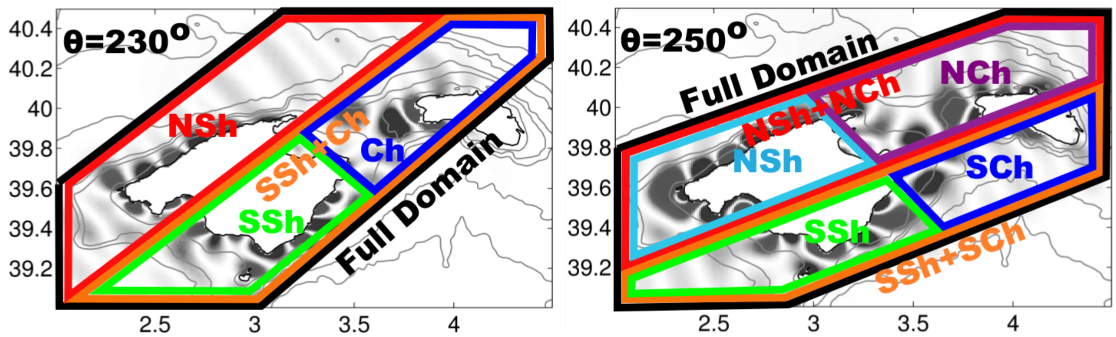

Figure 4: Gravity wave forcing scenarios. Each polygon depicts the domain of the passage of the synthetic gravity wave for $\theta = 230°$ (left panel) and $\theta = 250°$ (right panel). Polygon name abbreviations are as follows: Full Domain - full forcing domain, NSh - northern shelf, SSh - southern shelf, Ch - entire Channel, NCh - northern part of the Channel, SCh - southern part of the Channel.

3.2. The role of the Mallorca shelves and Menorca Channel

To quantify the shelves' and Channel's contributions to the meteotsunami amplification prior to the impact in Ciutadella harbour, a number of scenarios were run with the aim of exciting different subregions of the domain separately and exclusively. These synthetic forcing scenarios are depicted in Figure 4. During each forcing scenario the gravity wave was allowed to propagate only over the respective part of the domain. Gravity wave amplitudes rose linearly in time from zero to 3 hPa for 8 model timesteps and they were spatially smoothed at the relevant subdomain boundaries over the two outermost modeling cells to reduce sharp atmospheric pressure gradients. We chose angles and speeds which were shown to generate maximum rissaga in Ciutadella (see Figure 2), namely $\theta = 230°$ forcing (Figure 4, left panel) with gravity wave speeds $U = 28$ m/s and $U = 35$ m/s, and $\theta = 250°$ forcing (Figure 4, right panel) with speeds $U = 35$ m/s. Note that the $\theta = 230°$ forcing is aligned roughly with the isobaths of the southern shelf, while $\theta = 250°$ forcing is aligned with the isobaths of the northern shelf, see Figure 3. Results of these simulations are shown in Table 3.2. For each scenario, the maximum sea level anomaly is also provided as the percentage of the maximum anomaly obtained when exciting the whole continental shelf domain.

During the ($\theta = 230°, 28$ m/s) forcing scenario the Channel excitation is the most important one - we can generate 93% of the full forcing (Full Domain) response by forcing the Channel alone (Ch scenario). The difference is minimal between Ch and SSh+Ch forcing scenarios, indicating that the contribution of the southern Mallorca shelf is minimal in the build-up of the SSH anomaly. Moreover, exciting only the shelf, either northern or southern, does not lead to significant SSH anomalies in Ciutadella. The same qualitative results are obtained with faster waves in the ($\theta = 230°, 35$ m/s) forcing scenario. The Channel is still of paramount importance (97%). The northern shelf has greater importance - we generate 28% of the full response by exciting the northern shelf and 24% of the full response by exciting the southern one, but neither of them gives rise to significant rissagas when excited separately. While the Proudman resonance over the steeper northern shelf becomes more important for faster gravity waves, the Channel is still the key region where critical amplification takes place. The impact of deeper waters off the northern shelf is also visible for the ($\theta = 250°, 35$ m/s) forcing scenario, where the excitation over the northern shelf and the northern part of the Channel (NSh+NCh) generates 81% of the full response, while forcing over the northern part of the Channel alone (NCh) generates 73% of the full response. The contribution of the northern shelf is still low but relatively larger than in previous cases with $\theta = 230°$ forcing. Southern shelf and southern part of the Channel (SSh+SCh) generate about 31% of the full response while southern part of the Channel (SCh) generates 30% of the full response. The main conclusion of these experiments is that the key region that must be atmospherically excited to produce a strong rissaga is almost exclusively the Channel itself.

As mentioned already in Section 3.1, the shelves therefore serve merely as wave guides for barotropic meteotsunami waves into the Channel but do not contribute significantly to the magnitude of the final SSH oscillation in Ciutadella. From a practical operational point of view this means that pressure anomalies, generated very locally only over the Channel, may lead to substantial rissagas.

θ, U	**Full Domain**	**SSh+Ch**	**SSh**	**Ch**	**NSh**		
$230°, 28$ m/s	1.64 m	1.56 m (95%)	0.28 m (17%)	1.54 m (93%)	0.17 m (10%)		
$230°, 35$ m/s	1.56 m	1.56 m (100%)	0.37 m (24%)	1.51 m (97%)	0.44 m (28%)		
θ, U	**Full Domain**	**SSh+SCh**	**SSh**	**SCh**	**NSh+NCh**	**NSh**	**NCh**
$250°, 35$ m/s	1.83 m	0.56 m (31%)	0.40 m (22%)	0.54 m (30%)	1.49 m (81%)	0.33 m (18%)	1.34 m (73%)

Table 1: Maximum SSH anomaly in Ciutadella during different forcing scenarios, shown in Figure 4. The elevations are in meters, percentages below each value are proportions to the maximum anomaly from Full Domain forcing scenario.

Such was, for example, the event on the August 18th 2014: a passage of a single convective nucleus generated a very local pressure oscillation of 2.5 hPa in Ciutadella (light blue line in Figure 5) which was entirely absent in the measurements in Pollença and other points of the island of Mallorca, as shown in Figure 5, but nevertheless generated a peak-to-peak 1.45 m rissaga in Ciutadella (not shown in this paper, see [23]). As shown by thermal IR satellite image analysis in [23], the nucleus appeared in southern Mallorca and travelled across Mallorca and the Menorca Channel to reach Ciutadella at the time of the pressure oscillation which is also the time of the main sea level oscillation (not shown). With the available data there is no way of proving that the convective nucleus was generating the same kind of pressure oscillation along all its track but the constant appearance (size, shape and intensity) from the satellite images suggests that no important changes were occurring. Pressure oscillation linked to a higly localized convective nucleus has induced a significant marine response as the nucleus crossed the Menorca Channel at $\theta = 230 - 240°$ direction with $U = 27 - 28$ m/s speed.

This kind of evolution presents a serious challenge for the current Balearic observation system since it dramatically reduces effective warning times and

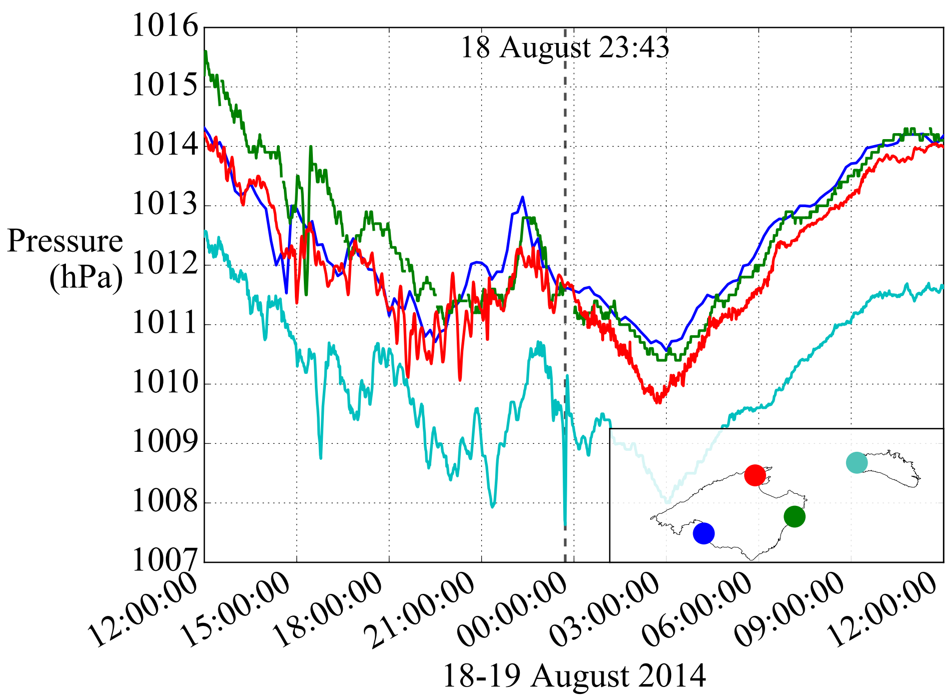

Figure 5: Air pressure [hPa] during a single and highly localized pressure oscillation occuring at Ciutadella (light blue line), generating a 1.45 m rissaga in the harbour. The oscillation was completely absent at Pollença (red line) and other pressure sensor locations on Mallorca (green and blue lines). See colored circles in the inset map for sensor locations.

indicates that, when too sparse, air pressure observations over Mallorca are not always an infallible criterion for *dismissing* the rissaga occurence. Until a denser grid of (inland and offshore) air pressure stations is facilitated, the atmospheric model capability of timely forecasting the appearance of an atmospheric disturbance, however difficult this may be, could be of importance to anticipating a meteotsunami arrival.

3.3. Propagation Paths and Speeds in the Menorca Channel: Forced and Free Waves.

To further understand the interplay between the atmospheric forcing and ocean bathymetry, we investigated how meteotsunamis propagate over the Menorca

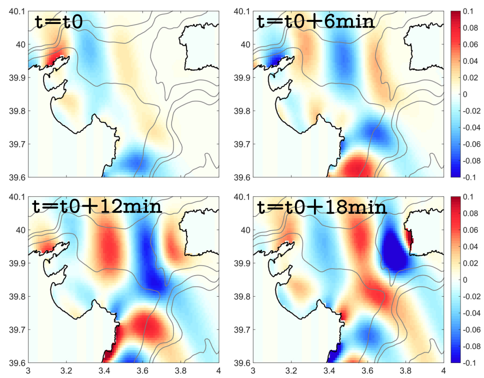

Figure 6: Meteotsunami focusing on Menorca Channel bathymetry. Panels show snapshots of SSH anomaly field [m] as meteotsunamis, arriving from northern and southern shelf, converge over the Channel towards Ciutadella. The colorscale has been limited to ±0.1 m to enhance visibility. Plots depict the $U = 28$ m/s gravity wave forcing scenario.

Channel at forcing velocities $U = 22, 26, 28, 30, 34$ m/s and gravity wave incident angle $\theta = 230°$. Figure 6 shows that the Channel bathymetry acts as a focusing lens for the two meteotsunami waves coming from the northern and southern shelf. Waves from the southern shelf propagate along its general direction and traverse the Channel straight towards Ciutadella. Waves from the northern shelf are on the other hand deflected from the along-shelf direction by the shallow Channel bathymetry, turning them towards Ciutadella. Figure 6 depicts four SSH anomaly snapshots where focusing and amplification of northern and southern meteotsunami branches are visible. Meteotsunami tracks converge along the Channel isobaths and merge prior to entering the Ciutadella harbour.

Proudman resonance influence on the propagation path can be evaluated by tracking the maximum SSH anomaly trajectories from both (northern and southern) meteotsunami branches, shown in Figure 6, as they travel across the Channel. These tracks are shown in Figure 7. As expected, the resonance plays a significant role: faster meteotsunamis traverse the Channel over a larger mean depth $\langle H \rangle_L$ which was estimated as a length-averaged line integral of ocean depth over the respective trajectory $\langle H \rangle_L = \Lambda^{-1} \int_L H(l) dl$, where $\Lambda = \int_L dl$ is the trajectory length and $H(l)$ is the model bathymetry value at location l along the corresponding path L (colored curves in Figure 7), obtained at forcing speed U. A meteotsunami, generated by the $U = 22$ m/s gravity wave, traverses the Channel over the ocean region with a mean depth of 69.8 m. A meteotsunami, generated by the $U = 34$ m/s gravity wave, on the other hand propagates over the Channel at a mean depth of 76.4 m, see $\langle H \rangle_L$ in the legend of Figure 7.

Meteotsunami speeds were estimated from the maximum SSH anomaly trajectories across the Menorca Channel. These results are presented in Figure 8 which depicts how the mean modelled meteotsunami speed (dark blue circles) varies with the atmospheric gravity wave speed and barotropic speed over its propagation path. As expected, in the subcritical forcing regime $U < c_{b0}$ the sea surface displacement $\eta(x,t)$ also propagates with the speed U, since it can be expressed as

$$\eta(x,t) = -\frac{\delta p}{\rho g} \cdot \frac{x - Ut}{1 - (U/c_{b0})^2}\,, \tag{1}$$

where δp is the amplitude of the pressure perturbation, ρ is sea water density, g is acceleration due to gravity, and x and t are spatial and time coordinates, respectively [24].

If however the atmospheric gravity wave is supercritical ($U > c_{b0}$) then modelled meteotsunamis propagate faster than barotropic free waves but slower than the atmospheric gravity wave (see dark blue circles in the $U > c_{b0}$ region of Figure 8). A first order explanation of this behaviour is as follows. It has been shown [24] that when a supercritical storm, simulated as a Gaussian packet pressure perturbation of velocity $U > c_{b0}$, crosses a topographic obstacle, it generates a forced ocean wave, propagating with the storm velocity U, but also transmitted and reflected barotropic transient wake packets propagating with the local barotropic velocities. A supercritical air pressure wave train, crossing the Menorca Channel, will consequently radiate forced and transient barotropic waves, most notably a forced supercritical ocean wave, propagating as $\sin(x - Ut)$, x being distance along the direction of the gravity wave, and a continuous superposition of transient barotropic wake waves, generated continuously as the atmospheric gravity wave passes ocean regions of depths $H(x)$, each propagating

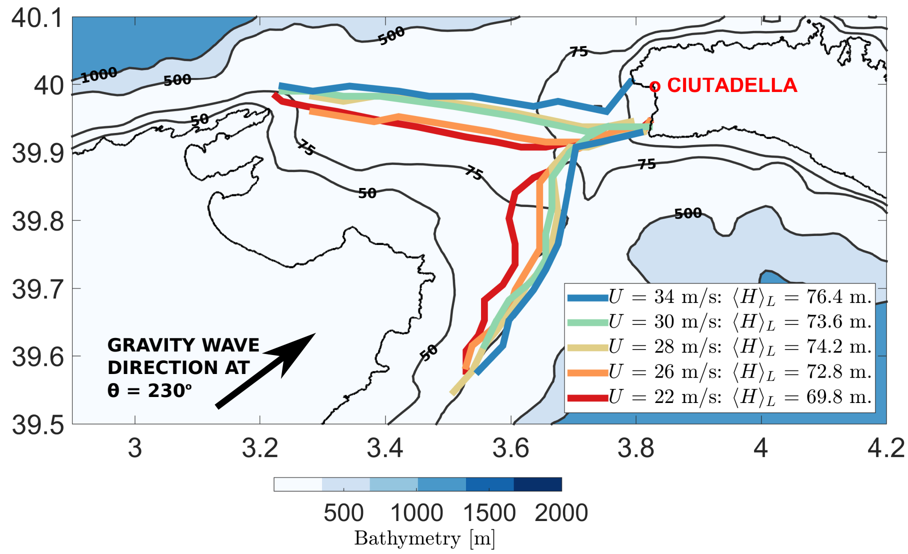

Figure 7: Maximum SSH anomaly trajectories across the Menorca Channel (colored curves) for different gravity wave speeds U at $\theta = 230°$. Quantity $\langle H\rangle_L$ in the Figure legend denotes average depth along each respective trajectory L. Blue shades with dark grey contours denote the model bathymetry [in meters]. Lateral angular width of the meteotsunami forcing was $1°$.

roughly along the forcing direction as $\sin(x - \sqrt{gH(x)}t)$.

To get an estimate of the meteotsunami velocity along the forcing direction, we approximate the superposition of wake waves with a single wave $\sin(x - \langle c_b\rangle_L t)$, travelling at the mean barotropic speed $\langle c_b\rangle_L$ along the path of the meteotsunami propagation. Mean barotropic speed is estimated as a distance-averaged line integral of $\sqrt{gH}$ over the meteotsunami propagation contour L (these propagation and integration contours are shown as colored curves in Figure 7):

$$\langle c_b\rangle_L = \Lambda^{-1}\int_L \sqrt{gH(l)}dl\,. \tag{2}$$

The superposition of the forced and barotropic waves then simplifies to

$$\sin(x - Ut) + \sin(x - \langle c_b\rangle_L t) = \tag{3}$$

$$= 2\cos\left[\frac{U - \langle c_b\rangle_L}{2}t\right]\sin\left[x - \frac{U + \langle c_b\rangle_L}{2}t\right].$$

The cosine term above denotes temporal modulation of the superposition amplitude (and becomes a unit constant at the Proudman resonance where $U = \langle c_b\rangle_L$). The sine term above implies that the meteotsunami propagates with a velocity which is to a first order equal to the average of the atmospheric wave velocity and mean barotropic velocity along its path:

$$\tilde{c}_L = \frac{U + \langle c_b\rangle_L}{2}. \tag{4}$$

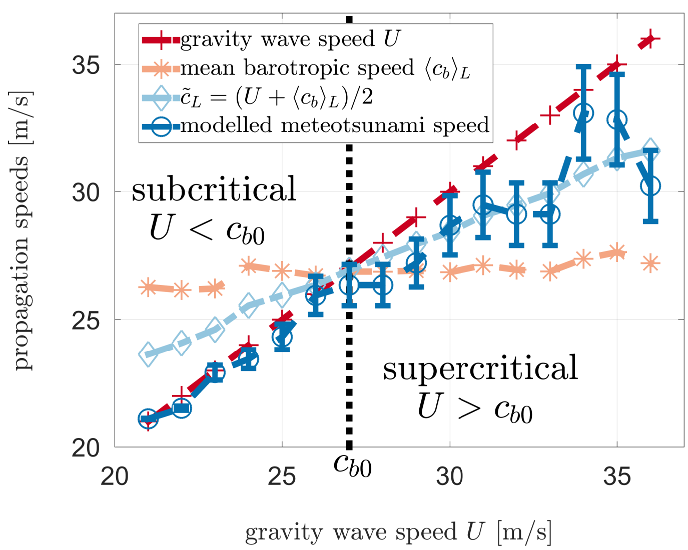

Figure 8: Mean propagation speeds along the maximum SSH anomaly trajectories for different gravity wave speeds U at $\theta = 230°$. Red color: air pressure gravity wave speeds U. Beige color: mean barotropic speeds computed along the trajectory of meteotsunamis, generated by the gravity waves of velocities U. Light blue color: $\tilde{c}_L = (U + \langle c_b\rangle_L)/2$, the average of both speeds. Dark blue color: the modelled meteotsunami propagation speeds along the forcing direction, obtained by directly tracking the meteotsunamis in the simulation results. Vertical dashed black line marks Menorca Channel barotropic speed $c_{b0} \approx 27 - 28$ m s^{-1}, delimiting sub- and supercritical forcing regimes.

Note that at the Proudman resonance $\tilde{c}_L$ equals U as it should. Equation

(4) explains why the modelled meteotsunami speed values (dark blue circles in Figure 8) are faster than barotropic (beige symbols in Figure 8) and slower than forcing speeds (red symbols in Figure 8). Error bars in Figure 8 are our estimates of the errors in tracked meteotsunami speeds, rising from 1 percent at 21 m s^{-1} to 5 percent at 36 m s^{-1}. This drop in accuracy is due to the fact that faster waves tend to exhibit spatially spread front-like maxima patterns in the Channel as they approach Menorca (not shown), making the possible location, and hence the computed propagation speed of the meteotsunami somewhat smeared in space. It is nevertheless clear that supercritical meteotsunamis travel with velocities below the forcing speed U and above the local barotropic speed, as indicated by the derived relationship (4), which arises out of the wave nature of the forcing as the propagation speed of the superimposed forced waves and free barotropic wake waves. (An interesting case of an actual occurence of the superposition of forced and free waves, leading to the great Adriatic surge of 1978, has been described in [25].)

4. Conclusions

An array of numerically generated atmospheric gravity wave trains was used to investigate Balearic meteotsunami generation, amplification and propagation. A sensitivity study of meteotsunami amplitude inside and outside Ciutadella harbour was performed in a similar fashion to [6], indicating that a wide range of gravity wave speeds ($23 - 36$ m/s) and angles of propagation ($210 - 250°$) may lead to substantial meteotsunami generation. The above speed and angle ranges were accounted for by the regional orientation and shape of the Balearic bathymetry which determine where the Proudman resonance may occur.

To quantify shelf and Channel contributions to meteotsunami intensity, we ran a set of simulations with forcings constrained to localized and isolated subregions of the modelling domain. These simulations indicate that in order to generate a significant meteotsunami, the Channel has to be atmospherically excited. Excitations over the northern and sourthern Mallorca shelves alone are not capable of generating destructive meteotsunamis. The shelves serve mostly as waveguides, leading meteotsunami waves along the Mallorca coast and into the Channel where they get amplified by the atmospheric forcing over the Channel, if such forcing is present. This means that very locally induced pressure oscillations, arising from atmospheric instabilities over the Menorca Channel alone, can lead to significant meteotsunamis as well. Such events have indeed occured and one such observation is provided. Such atmospheric scenarios, rare as they may be, seriously reduce lead times for any early warning observation system in Mallorca. Numerical modelling capabilities to forecast (or at least indicate a significant possibility of) meteotsunami occurences at least a day in advance could therefore be important for the prevention and mitigation of the consequences of such events. This provides further motivation for complementing existing observational networks and meteotsunami alert systems with numerical modelling systems.

If the gravity waves propagate over the Balearic region from the southeast, then the Channel bathymetry is shown to act as a focusing lens for the corresponding meteotsunami waves. These waves propagate along the Channel isobaths and focus just prior to the impact with Ciutadella harbour. It is further demonstrated that maximum SSH anomalies, generated by faster atmospheric gravity waves, propagate over deeper ocean regions, as one would expect from the Proudman resonance.

We have further investigated meteotsunami propagation under sub- and supercritical atmospheric forcing. Subcritical atmospheric gravity waves generate meteotsunamis which propagate over the Menorca Channel with velocity U. Meteotsunamis created by supercritical atmospheric gravity waves on the other hand propagate with velocity $\tilde{c}_L = (U + \langle c_b \rangle_L)/2$ which is, to the first order, an average of the gravity wave speed U and the barotropic speed of the wake wave, as shown in Figure 8, implying that, unlike subcritical meteotsunamis, these are not free barotropic but rather forced waves arising from an interplay of influences by forcing and the bathymetry. The relationship $\tilde{c}_L = (U + \langle c_b \rangle_L)/2$ arises out of the wave nature of the atmospheric forcing and turns out to be a consequence of the superposition between supercritically forced ocean waves and barotropic ocean wake waves.

Acknowledgments. We are grateful to John Allen and Evan Mason for kindly proof-reading and otherwise discussing the manuscript. We sincerely thank anonymous reviewers for their suggestions which led to a much improved paper.

Author contributions. C. T. and A. K. analysed the observational data upon which synthetic gravity wave forcing was generated. B. M. maintained the modelling environment and performed the simulations. M. L., B. M. and C. T. created the figures. M. L. and B. M. prepared synthetic atmospheric boundary conditions for ROMS, performed post-processing analyses and wrote the paper. A. J. provided the analysis for the August 19th 2014 event. C.T., A.K., B.M., M.L. and J.T. devised the research plan. All authors contributed to the final version of the manuscript. M. L. and B. M. contributed equally to this research.

Funding. This research did not receive any specific grant from funding agencies in the public, commercial, or not-for-profit sectors.

References

[1] S. Monserrat, I. Vilibić, A. B. Rabinovitch, Meteotsunamis: Atmospherically Induced Destructive Ocean Waves in the Tsunami Frequency Band, Natural Hazards and Earth System Sciences 6 (2006) 1035–1051. doi:10.5194/nhess-6-1035-2006.

[2] I. Vilibić, J. Šepić, A. B. Rabinovitch, S. Monserrat, Modern Approaches in Meteotsunami Research and Early Warning, Frontiers in Marine Science 3:57 (2016) 1–7. doi:10.3389/fmars.2016.00057.

[3] L. Renault, G. Vizoso, A. Jansà, J. Wilkin, J. Tintoré, Toward the Predictability of Meteotsunamis in the Balearic Sea using Regional Nested Atmosphere and Ocean Models, Geophysical Research Letters 38 (2011) L10601. doi:10.1029/2011GL047361.

[4] J. Šepić, I. Vilibić, A. B. Rabinovitch, S. Monserrat, Widespread Tsunami-like Waves of 23-27 June in the Mediterranean and Black Seas generated by High-Altitude Atmospheric Forcing, Scientific Reports 5 (2015) 11682. doi:10.1038/srep11682.

[5] A. B. Rabinovich, Seiches and Harbour Oscillations., in: Y. C. Kim (Eds.), Handbook of Coastal and Ocean Engineering, World Scientific Publ., 2009, pp. 193–236.

[6] I. Vilibić, S. Monserrat, A. Rabinovich, H. Mihanović, Numerical Modelling of the Destructive Meteotsunami of 15 June, 2006 on the Coast of the Balearic Islands, Pure and Applied Geohysics 165 (2008) 2169–2195. doi:10.1007/s00024-008-0426-5.

[7] C. Ramis, A. Jansà, Condiciones metreorologicas simultaneas a la aparicion de oscilaciones del nivel del mar de amplitude extraordinaria en el Mediterraneo occidental, Revista de Geofísica 39 (1983) 35–42.

[8] J. Tintoré, D. Gomis, S. Alonso, D. P. Wang, A theoretical study of large sea level oscillations in the western Mediterranean, Journal of Geophysical Research 93 (1988) 10797–10803. doi:10.1029/JC093iC09p10797.

[9] D. Gomis, J. Tintoré, S. Monserrat, Pressure-forced seiches of large amplitude in inlets of the Balearic Islands, Journal of Geophysical Research 98 (1993) 14437–14445. doi:10.1029/93JC00623.

[10] A. Jansà, S. Monserrat, D. Gomis, The rissaga of 15 June 2006 in Ciutadella (Menorca), a meteorological tsunami, Advances in Geosciences 12 (2007) 1–4. doi:10.5194/adgeo-12-1-2007.

[11] I. Vilibić, J. Šepić, Destructive Meteotsunamis along the Eastern Adriatic Coast: Overview, Physics and Chemistry of the Earth 34 (2009) 904–917. doi:10.1016/j.pce.2009.08.004.

[12] J. Šepić, I. Vilibić, S. Monserrat, Teleconnections between the Adriatic and the Balearic Meteotsunamis, Physics and Chemistry of the Earth 34 (2009) 928–937. doi:10.1016/j.pce.2009.08.00.

[13] A. B. Rabinovitch, S. Monserrat, I. V. Fain, Numerical modeling of extreme seiche oscillations in the region of the Balearic Islands, Oceanology 39 (1999) 16–24.

[14] M. Marcos, S. Monserrat, R. Medina, C. Vidal, Influence of the atmospheric wave velocity in the coastal amplification of meteotsunamis., in: A. Yalciner, E. N. Pelinovsky, C. Synolakis, E. Okal (Eds.), Submarine Landslides and Tsunamis, Vol. 12, Kluwer Acad. Publ., 2003, pp. 247–253.

[15] P. Whitmore, B. Knight, Meteotsunami forecasting: sensitivities demonstrated by the 2008 Boothbay, Maine, event, Natural Hazards 74 (2014) 11–23. doi:10.1007/s11069-014-1056-0.

[16] J. Šepić, I. Vilibić, I. Fine, Northern Adriatic meteorological tsunamis: Assessment of their potential through ocean modelling experiments, Journal of Geophysical Research: Oceans 120 (2015) 2993–2310. doi:10.1002/2015JC010795.

[17] S. Monserrat, A. Ibbetson, A. J. Thorpe, Atmospheric gravity waves and the Rissaga phenomenon, Quarterly Journal of Royal Meteorological Society 117 (1991) 553–570. doi:10.1002/qj.49711749907.

[18] S. Monserrat, A. J. Thorpe, Gravity-wave observations using an array of microbarographs in the Balearic Islands , Quarterly Journal of Royal Meteorological Society 118 (1992) 259–282. doi:10.1002/qj.49711850405.

[19] M. Marcos, S. Monserrat, R. Medina, A. Orfila, M. Olabarrieta, External forcing of meteorological tsunamis at the coast of the Balearic Islands, Physics and Chemistry of the Earth 34 (2009) 938–947. doi:10.1016/j.pce.2009.10.001.

[20] A. Shchepetkin, J. C. McWilliams, The Regional Oceanic Modeling System (ROMS): A Split-Explicit, Free-Surface, Topography-Following-Coordinate Oceanic Model, Ocean Modelling 9 (2005) 347–404. doi:10.1016/j.ocemod.2004.08.002.

[21] A. Orfila, S. Balle, G. Simarro, Topographic enhancement of long waves generated by an idealized moving pressure system, Scientia Marina 75 (2011) 595–603. doi:10.3989/scimar.2011.75n3595.

[22] J. Šepić, I. Medjugorac, I. Janeković, N. Dunić, I. Vilibić, Multi-Meteotsunami Event in the Adriatic Sea Generated by Atmospheric Disturbances of 25–26 June 2014, Pure and Applied Geophysics (2016) 1–22. doi:10.1007/s00024-016-1249-4.

[23] A. Jansà, Rissagues: El caso de 19 de Agosto de 2014, Tiempo y Clima 46 (2014) 43–48. doi:N/A.

[24] R. Vennell, Long Barotropic Waves Generated by a Storm Crossing Topography , Journal of Physical Oceanography 37 (2007) 2809–2823. doi:10.1175/2007JPO3687.1.

[25] M. Orlić, D. Belušić, I. Janeković, M. Pasarić, Fresh evidence relating the great Adriatic surge of 21 June 1978 to mesoscale atmospheric forcing, Journal of Geohysical Research: Oceans 115 (2010) 2156–2202. doi:10.1029/2009JC005777.